



Review

# Geochemical and Physical Methods for Estimating the Saturation of Natural Gas Hydrates in Sediments: A Review

Yuan Xue <sup>1</sup>, Hailong Lu <sup>1,2,\*</sup>, Hailin Yang <sup>1</sup> , Wenjiu Cai <sup>1,3</sup>  and Linsen Zhan <sup>1</sup>

<sup>1</sup> Beijing International Center for Gas Hydrate, School of Earth and Space Sciences, Peking University, Beijing 100871, China; ritaxuey@stu.pku.edu.cn (Y.X.); yanghailin@pku.edu.cn (H.Y.); caiwenjiu@pku.edu.cn (W.C.); zhanlinsen@pku.edu.cn (L.Z.)

<sup>2</sup> National Engineering Research Center for Gas Hydrate Exploration and Development, Guangzhou 511466, China

<sup>3</sup> School of Environment and Energy, Peking University Shenzhen Graduate School, Shenzhen 518055, China

\* Correspondence: hlu@pku.edu.cn

**Abstract:** The saturation of natural gas hydrates is a key parameter for characterizing hydrate reservoirs, estimating hydrate reserves, and developing hydrate as an energy resource. Several methods have been proposed to estimate hydrate saturation, although most of these studies rely on logging and seismic data. However, the methods for estimating hydrate saturation from recovered core sediments have not been thoroughly reviewed, which hinders a deeper understanding, proper application, and the use of these experimental data to integrate geophysical and numerical model results with the actual geological conditions. In this paper, the methods widely used for estimating natural gas hydrate saturation from core sediments, including those based on pore water chemistry ( $\text{Cl}^-$  concentration,  $\delta\text{D}$ , and  $\delta^{18}\text{O}$  values), gas volumetric analysis, and temperature anomaly, have been summarized in terms of the principle, estimation strategy, and issues to be considered of each method. The applicability, advantages and disadvantages, and scope of application of each method are also compared and discussed. All methods for estimating gas hydrate saturation have certain limitations. A comprehensive application of results from multiple methods could lead to a better understanding of the amount of gas hydrate in sediments, although the chlorinity of pore water is the most commonly used method of estimation.

**Keywords:** hydrate saturation; pore water chlorinity; isotope; volumetric method; infrared temperature



**Citation:** Xue, Y.; Lu, H.; Yang, H.; Cai, W.; Zhan, L. Geochemical and Physical Methods for Estimating the Saturation of Natural Gas Hydrates in Sediments: A Review. *J. Mar. Sci. Eng.* **2024**, *12*, 1851. <https://doi.org/10.3390/jmse12101851>

Academic Editor: Anabela Oliveira

Received: 11 September 2024

Revised: 11 October 2024

Accepted: 15 October 2024

Published: 16 October 2024



**Copyright:** © 2024 by the authors. Licensee MDPI, Basel, Switzerland. This article is an open access article distributed under the terms and conditions of the Creative Commons Attribution (CC BY) license (<https://creativecommons.org/licenses/by/4.0/>).

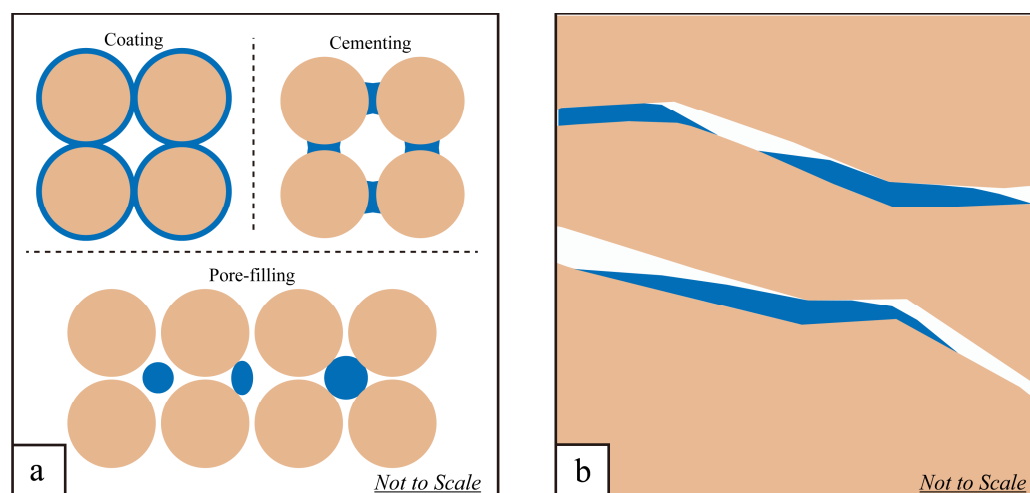
## 1. Introduction

Gas hydrates are ice-like caged compounds formed by guest molecules (the dominant guest molecule in nature is methane) and water molecules at low temperatures and high pressures [1]. Gas hydrates are extensively distributed in nature, generally in underground permafrost [2] and marine sediments [3]. The saturation of natural gas hydrate is a key parameter for assessing the resource potential of a hydrate reservoir [4,5]. In sediments, the saturation of gas hydrate ( $S_h$ ) is defined as the ratio of the volume of gas hydrate to the pore volume of the sediments, as shown in Equation (1).

$$S_h = \frac{\text{the volume of gas hydrate}}{\text{the pore volume of sediments}} \quad (1)$$

The saturation of gas hydrate should only refer to the hydrates that are relatively homogeneously distributed in sediments. In marine sediments, the morphologies of natural gas hydrate hosting patterns are generally classified into two types [6]. The first type involves hydrates that are relatively homogeneously distributed in pores of sediments (Figure 1a). Some studies have suggested that these hydrates may exist as coatings, cements, or fillings in intergranular spaces, etc., but the actual morphology in natural sediment pores

remains undetermined [7,8]. The second type encompasses hydrates that appear in vein-like, nodule-like, lens-like forms, etc., which are randomly distributed along faults or fractures and exhibits irregular shapes and sizes ranging from a few millimeters to several tens of centimeters (Figure 1b) [9–11]. Such features of these fracture-filling hydrates make it impossible to calculate the saturation. Although some studies have used the volume of hydrate collected relative to the total volume of sediment samples to quantify the abundance of fracture-filling hydrates, the value obtained can only be applied to a small range of sediments [12].



**Figure 1.** Morphologies of natural gas hydrates in sediments: (a) pore-filling hydrates, existing in sediment pores; (b) fracture-filling hydrates, randomly distributed along faults or fractures. The dark blue color represents gas hydrates, while the brown color denotes sediments.

Natural gas hydrate in marine sediments is frequently associated with free gas [13,14]. However, current sampling methods cannot guarantee that samples are strictly preserved in their original, intact state. It is difficult to separate free gas from hydrate-derived gas, and geophysical methods can only roughly discern between the two [15]. Consequently, the gas volume measured from cores may represent a mixture of hydrate-derived gas and free gas. Distinguishing between free gas and natural gas hydrates is complex and beyond the scope of this paper. It is generally assumed that any free gas in the cores has leaked, and that the gas collected originates from hydrate dissociation. Moreover, free gas occupies a portion of the pore space in the sediment, thereby affecting the calculation of hydrate saturation.

The accurate prediction of gas hydrate saturation is critical for reserve estimation. Exploiting reservoirs with high hydrate saturation offers greater economic potential [16]. Previous studies have estimated hydrate saturation in various regions, such as the Nankai Trough [17,18], Ulleung Basin [19], Mount Elbert [20], Mallik [21], Bay of Bengal [22], Black Sea [23], and South China Sea [5,16,24], providing valuable references for subsequent research and production activities. Hydrate saturation can be estimated using non-core geophysical methods, including seismic velocity and certain logging parameters (e.g., sonic velocity, electrical resistivity, etc.), or through the direct analysis and testing of core samples obtained via drilling (e.g., pore water freshening, isotope anomaly, etc.) [6,25–27]. Geophysical methods are convenient and cost-effective, making them suitable for preliminary large-scale exploration; however, they are subject to method-associated uncertainties [28–30]. Basically, the direct analysis of hydrate-bearing sediment cores can yield relatively reliable saturation values and serve as an accurate reference for calibrating saturation values derived from geophysical methods such as well logging [16,31], although it is difficult to collect intact hydrate samples. When core samples are well-preserved and the hydrate has not dissociated, saturation can be determined by collecting hydrate-derived gas directly through core degassing. For core samples in which hydrate has dissociated, hydrate sat-

uration can be estimated at the end of hydrate dissociation using geochemical proxies or temperature anomalies.

Currently, while summaries of geophysical and numerical simulation techniques for estimating natural gas hydrate saturation exist, there is a notable lack of reviews on methods for determining hydrate saturation in core sediment samples. This paper provides a comprehensive review of several widely utilized methods for estimating hydrate saturation in sediments: the pore water chemistry-based ( $\text{Cl}^-$ ,  $\delta^{18}\text{O}$  and  $\delta\text{D}$ ) method, the gas volumetric method, and the temperature anomaly-based method. Section 2 elucidates the principles underlying these methods, emphasizing their reliance on the intrinsic properties of hydrates, such as the structure of hydrate water cages, the hydration number ( $n$ ), the patterns of temperature changes in the hosting sediments, and the variations in  $\text{Cl}^-$  concentration and hydrogen and oxygen isotopes of pore water during hydrate formation and dissociation. Sections 3–5 focus on the specific calculations of saturation involved in pore-water geochemistry, gas volumetric analysis, and temperature anomaly detection, respectively, while also addressing the challenges and potential sources of error in each approach. Section 6 provides a comparison of the applicability, as well as the advantages and disadvantages of each method, and identifies current deficiencies and gaps in the field. The paper concludes with a summary and recommendations for future research directions.

## 2. Basic Properties of Natural Gas Hydrate for Estimating Its Saturation in Sediments

### 2.1. Crystal Structure and Thermodynamic Properties of Natural Gas Hydrate

Natural gas hydrates are solid, non-stoichiometric compounds consisting of gas molecules and water, resembling ice crystals [1]. Water molecules form cage-like structures, enclathrating individual guest molecules within hydrogen-bonded cavities. The repulsion between the guest molecules and the surrounding water supports the formation of water cages of varying sizes. During hydrate formation, ions such as  $\text{Cl}^-$  and  $\text{Na}^+$  present in marine sediment pore water, as well as any molecules other than the guest molecules, are excluded from entering or participating in the formation of these water cages. The formation of hydrate water molecule cages is accompanied by the significant enrichment of heavy isotopes of oxygen and hydrogen, analogous to the isotope enrichment observed during ice formation. Studies have shown that the hydrogen bond lengths and far-infrared spectra of hydrate water molecule cages are also very similar to those found in ice [32]. Hydrate water cages are  $^{18}\text{O}$  and D-enriched, contributing to their greater energetic stability. The enthalpies of fusion of both  $\text{H}_2^{18}\text{O}$  and  $\text{D}_2^{16}\text{O}$  are higher than that of  $\text{H}_2^{16}\text{O}$ , and the melting temperatures of hydrates containing  $\text{D}_2\text{O}$  are higher compared to those containing  $\text{H}_2\text{O}$  for the same guest molecules [33,34].

The number of water molecules per hydrate unit is referred to as the hydration number, denoted by  $n$ . For methane as the guest molecule, the hydrate can be represented as  $\text{CH}_4 \cdot n\text{H}_2\text{O}$ , where  $n$  indicates the moles of water associated with one mole of  $\text{CH}_4$  [35]. To date, three distinct crystal structures of natural gas hydrates have been identified [1]: Structure I, Structure II, and Structure H (Figure 2). The cubic structure I (sI-type) is the most common, with its unit cell consisting of eight water cages. Each cavity can host up to one guest molecule, linking eight guest molecules to the 46 water molecules in the sI-type unit cell (Figure 2). Methane hydrates typically form Structure I. When all water molecule cages are filled with methane, the stoichiometric ratio of  $\text{CH}_4$  to  $\text{H}_2\text{O}$  is 8:46, or 1:5.75, indicating a hydration number  $n = 5.75$  ( $\text{CH}_4 \cdot 5.75\text{H}_2\text{O}$ ) under conditions of full guest molecule occupancy. However, the hydration number of natural gas hydrates varies widely, as not all water molecule cages are necessarily fully occupied by gas, resulting in  $n$  values greater than 5.75. The precise measurement of the specific sample is required when using the parameter  $n$  in calculations, although Raman spectroscopy experiments have measured the hydration number  $n$  of methane hydrates under specific deep-sea temperature and pressure conditions to be 6.00 [35]. Cubic structure II (sII-type) unit cell consists of sixteen  $5^{12}$  cages (each water cage composed of 12 pentagonal faces) and eight  $5^{12}6^4$  cages (each comprising 12 pentagonal and four hexagonal faces), with a total of 46 water molecules per

unit cell. The guest molecules in sII-type hydrates are relatively larger than those in sI-type hydrates, typically including molecules such as propane (C<sub>3</sub>H<sub>8</sub>) and isobutane (i-C<sub>4</sub>H<sub>10</sub>). The hexagonal structure H (sH-type) unit crystal is composed of three 5<sup>12</sup> cages, two 4<sup>3</sup>5<sup>6</sup>6<sup>3</sup> cages, one 5<sup>12</sup>6<sup>8</sup> cage, and 34 water molecules. sH-type hydrates require combinations of both small and large guest molecules, such as methane with neohexane or methane with cycloheptane [36].

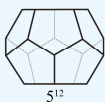
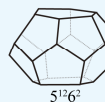
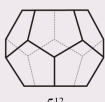

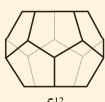
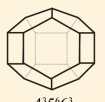
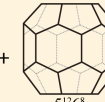
Structure type	Cavity types and number of cavities per unit cell	Number of water molecules per unit cell
sI	 ×2 +  ×6	46 H <sub>2</sub> O
sII	 ×16 +  ×8	136 H <sub>2</sub> O
sH	 ×3 +  ×2 +  ×1	34 H <sub>2</sub> O

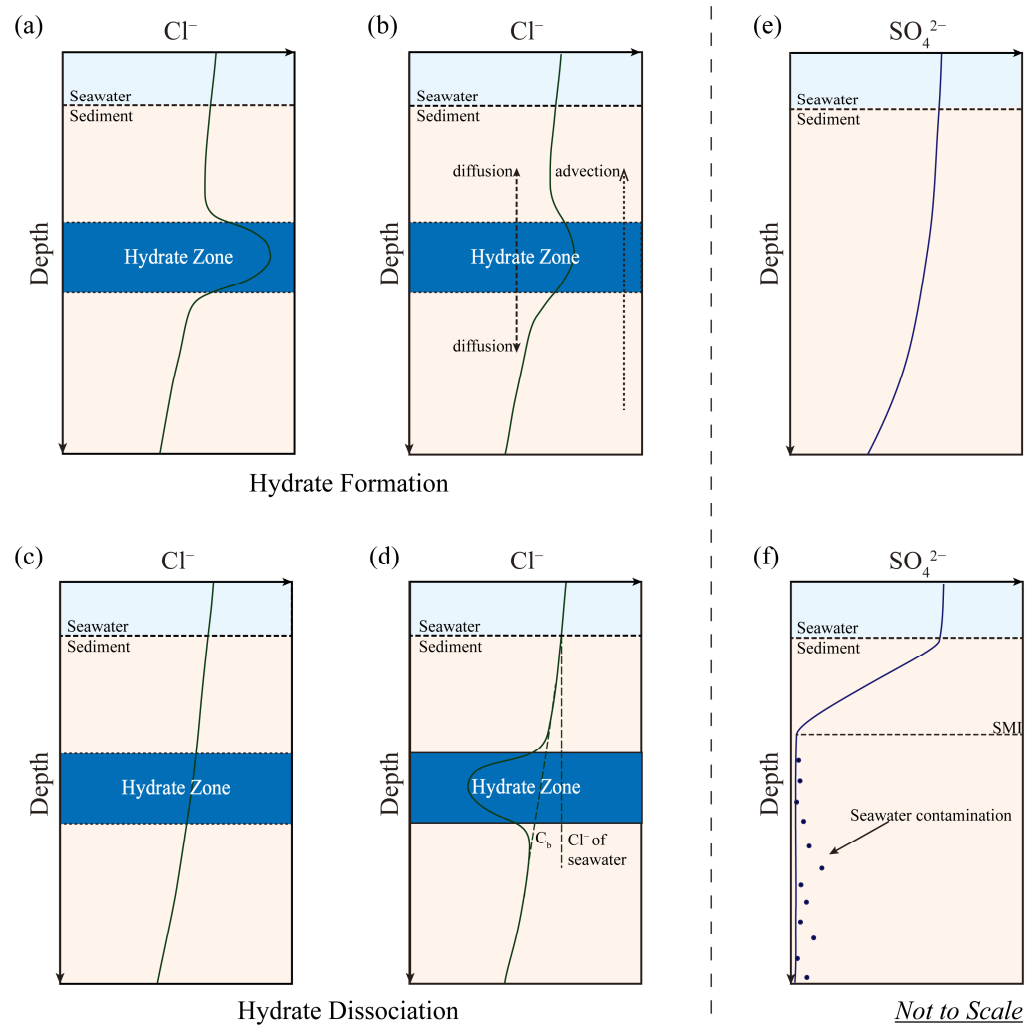
Figure 2. Three hydrate crystal structures.

### 2.2. Chemical and Physical Changes with Host Sediments by Hydrate Formation and Dissociation

The occurrence of natural gas hydrate is controlled by several factors, including temperature, pressure, chemical composition of pore water, gas components, and sediment properties [37,38]. At certain depths in marine sediments where the temperature and pressure fall within the stable regime of natural gas hydrate, hydrate can form when the concentration of natural gas (primarily methane) exceeds its saturation point [39–41]. Conversely, when the surrounding conditions change, such as through drilling disturbances, the temperature and pressure may deviate from the hydrate stability condition, leading to hydrate dissociation and associated alterations in the physical and chemical properties of the surrounding sediments.

Hydrate formation is an exothermic process, while its dissociation is endothermic, with the associated energy changes quantified by the enthalpy (heat) of formation and dissociation [36]. The dissociation enthalpy of methane hydrate in pure water and saline solutions, calculated using the Clausius–Clapeyron or Clapeyron equation, is approximately 50–60 kJ/mol [42]. Consequently, the dissociation of natural gas hydrates results in a decrease in the temperature of the surrounding sediments.

The formation or dissociation of hydrates also impacts the ion concentrations in pore water. During the formation of natural gas hydrates, water molecules from the surrounding pore water are incorporated into the hydrate lattice, a process that excludes ions, known as ion exclusion. Consequently, ions in the surrounding pore water become concentrated, resulting in elevated concentrations of Cl<sup>−</sup> and other ions (Figure 3a) [43–45]. Over time, the advection and diffusion of pore water in the sediment can reduce the concentration of Cl<sup>−</sup> (Figure 3b), potentially returning Cl<sup>−</sup> to its original concentration eventually (Figure 3c) [46,47]. If hydrate formation occurs at a very slow rate, the simultaneous advective and diffusive processes might alleviate or even negate the high Cl<sup>−</sup> concentration anomaly caused by ion exclusion. During hydrate dissociation, pure water is released from the hydrate, mixing with the surrounding pore water and reducing Cl<sup>−</sup> concentration (Figure 3d). This is referred to as the freshening effect. The hydrate saturation can be estimated from the deviation of the Cl<sup>−</sup> concentration from its original level in the pore water [45].



**Figure 3.** Profiles of ion concentrations in pore water under different conditions. (a) Increase in pore water  $\text{Cl}^-$  concentration at a specific depth due to ion exclusion during rapid hydrate formation. (b) Reduction in  $\text{Cl}^-$  concentration caused by pore water advection and diffusion. (c) Recovery of  $\text{Cl}^-$  concentration to its original level after an extended period of complete advective and diffusive processes in the pore water. (d) Decrease in pore water  $\text{Cl}^-$  concentration at a specific depth due to the freshening effect during hydrate dissociation. (e) A general profile of  $\text{SO}_4^{2-}$  concentration in pore water of sediments with scarce organic matter and an extremely low hydrocarbon flux. (f) A profile of  $\text{SO}_4^{2-}$  concentration in pore water of sediments with a certain content of organic matter and hydrocarbon flux.

During hydrate formation, heavy oxygen and hydrogen isotopes are preferentially incorporated into the solid phase (as detailed in Section 2.1), resulting in a depletion of  $^{18}\text{O}$  and D in the pore water [48]. Upon core retrieval, disturbances cause hydrate dissociation, releasing  $^{18}\text{O}$  and D into the pore water and increasing the  $\delta^{18}\text{O}$  and  $\delta\text{D}$  values. The degree of fractionation of oxygen or hydrogen isotope during hydrate formation in the hydrate-water system is expressed by the fractionation factor  $\alpha$  (Table 1). For comparison, the fractionation factor  $\alpha$  for ice formation in the ice-water system is also listed in Table 1. Generally, the enrichment factor  $\epsilon$  is used to calculate hydrate saturation, which indicates the degree of heavy isotope enrichment in the hydrate phase and is calculated from the fractionation factor  $\alpha$ , as shown in Equation (2). The isotopic composition of pore water

collected from gas hydrate-bearing sediments can provide information about the hydrate distribution and reservoir characteristics [49,50].

$$\varepsilon = \alpha - 1 \tag{2}$$

**Table 1.** Fractionation factor  $\alpha$  of O and H in hydrate-water and ice-water systems (modified from [50]).

System	$\alpha$ ( $^{18}\text{O}$ )	$\alpha$ (D)	Type	Solution	References
hydrate-water	1.0023–1.0032	1.014–1.019	sI	liquid water	[51]
	1.0024–1.0034	1.017–1.024	sI	saline NaCl sol.	[51]
	1.0034; 1.0037–1.0040		sI	natural pore water	[52]
	1.0028–1.0032		sI	3% NaCl sol.	[48]
	1.0024–1.0036		sI	natural pore water	[53]
	1.0025–1.0032	1.017–1.022	sII	liquid water	[51]
	1.0037		sII	THF sol.	[54]
	1.00268		sII	THF sol.	[32]
ice-water	1.0032				[54]
	1.0035 ± 0.0003				[55]
	1.0028	1.0206			[56]
	1.0029; 1.0031	1.0178; 1.0195			[57]
	1.00265	1.0195		dilute NaCl sol.	[58]
	1.00270	1.0203		sea water	[58]

### 3. Estimation of Hydrate Saturation from Pore Water Chemistry

Geochemical analysis of pore water can verify the presence of natural gas hydrates in complex sedimentary environments and quantify their saturation by examining the concentration of  $\text{Cl}^-$  and the values of  $\delta^{18}\text{O}$  or  $\delta\text{D}$  in pore water. These pore water chemical proxies need to be sampled and tested following hydrate dissociation.

#### 3.1. $\text{Cl}^-$ Concentration in Pore Water

##### 3.1.1. Basis of $\text{Cl}^-$ Concentration for Estimating Hydrate Saturation

Drilling cores from hydrate-bearing sediments disrupt the stability conditions of the hydrates, causing their dissociation. The negative anomaly in chloride ion concentration resulting from hydrate dissociation can be used to estimate hydrate saturation [59]. Chloride concentration serves as a reliable indicator since  $\text{Cl}^-$  does not typically participate in redox reactions or form precipitates in marine sediment environments [23]. Calculating hydrate saturation requires parameters such as the  $\text{Cl}^-$  concentration profile of pore water, the  $\text{SO}_4^{2-}$  concentration profile, and the associated volume change.

The concentration of  $\text{SO}_4^{2-}$  is utilized to correct for seawater contamination in the  $\text{Cl}^-$  concentration. In the pore water of sediments containing organic matter and hydrocarbon flux, the concentration of  $\text{SO}_4^{2-}$  rapidly decreases to zero at the sulfate–methane interface (SMI) due to the reduction of sulfate by upwelling methane (Figure 3f). The depth of the SMI marks the upper boundary of hydrate distribution. Below the SMI, the presence of  $\text{SO}_4^{2-}$  in pore water is considered to be a result of seawater contamination during coring. Therefore, the  $\text{Cl}^-$  concentration in pore water uncontaminated by seawater can be corrected by subtracting the  $\text{SO}_4^{2-}$  concentration below the SMI [59].

The degree of abnormal negative deviation in chloride concentration can serve as a proxy for the quantity of gas hydrate, necessitating an estimation of the background chloride profile [45]. If the  $\text{Cl}^-$  concentration in seawater was used as a background value, negative anomalies in  $\text{Cl}^-$  concentration deviating from the original background value would be observed at sediment depths, leading to inaccurate estimates of hydrate saturation (Figure 3f) [12]. The original baseline can be derived by extrapolating the chloride concentrations of pore water from non-hydrate zones in the same core [59,60] or by fitting a diffusion curve (Figure 3d) [12,61]. It should be noted that different fitting methods can yield varying results [60], which can be improved by considering the distribution of pore water and the diffusion context in a specific study area [23,62].



These discrete anomalies are used in Equations (3) and (4) to calculate the gas hydrate saturation value ( $S_h$ ) [23,59]:

$$M = 1 - \frac{C_h}{C_b} \quad (3)$$

$$S_h = \frac{\beta M}{1 + (\beta - 1)M} \quad (4)$$

Equations (3) and (4) can be combined into Equation (5) [61]:

$$S_h = \frac{\beta(C_b - C_h)}{C + \beta(C_b - C_h)} \quad (5)$$

In these equations, the parameter  $M$  represents the ratio of the dilution concentration caused by hydrate dissociation to the original pore water  $\text{Cl}^-$  concentration, where  $C_b$  is the in situ background pore water salinity, and  $C_h$  is the chloride concentration measured in core samples after the dissociation of the gas hydrate. The dimensionless constant  $\beta$  quantifies the density and volume changes resulting from the dissociation of natural gas hydrates and is related to the hydration number  $n$  of the hydrates, the density of the hydrates, and the density of the pore water [23,59]. The  $\beta$  value is reported as 1.257 in [47] and 1.27 in [59,63]. Ultimately, the gas hydrate saturation value  $S_h$  is determined.

### 3.1.2. Factors Affecting the Estimation of Hydrate Saturation with $\text{Cl}^-$

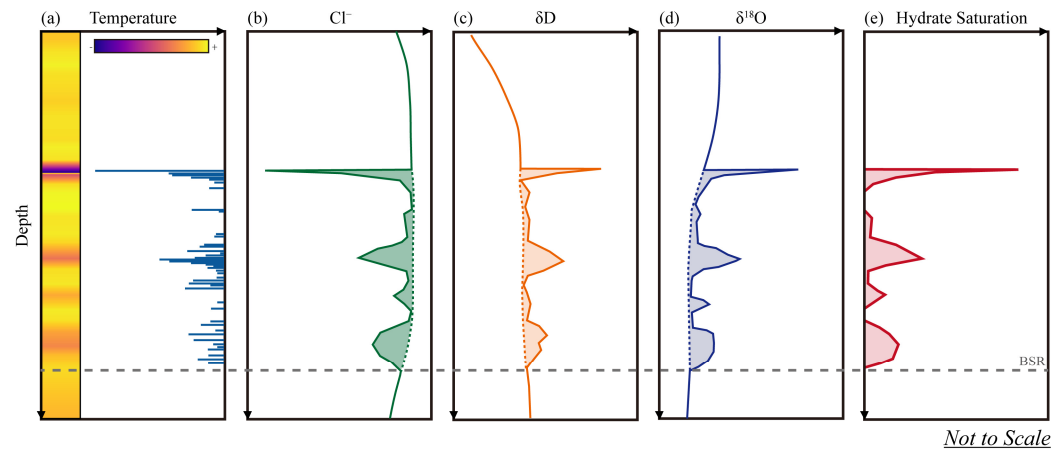
The accurate determination of chloride ion concentration is fundamental for obtaining reliable hydrate saturation values. During pore water extraction from sediments, it is essential to avoid any contamination [64]. The previously mentioned sulfate concentration in pore water can help identify seawater contamination experienced during drilling and core retrieval, and it can be further used to estimate the extent of seawater contamination.

Certain marine processes may affect the accuracy of the  $\text{Cl}^-$  method for estimating hydrate saturation. Previous studies have noted that chloride enrichment requires months or even years to return to background values through diffusion [46]. If the  $\text{Cl}^-$  outside the hydrate crystals has not yet fully diffused to reach a steady state, the estimation of the  $\text{Cl}^-$  baseline ( $C_b$ ) will be inaccurate, which, in turn, affects the estimation of gas hydrate saturation [59]. The  $\text{Cl}^-$  concentration of the hydrate undergoing formation cannot be used as a proxy for saturation calculation, as the ion exclusion process during hydrate formation may overprint and offset the freshening process associated with hydrate dissociation during coring [23]. In certain unique depositional environments, the negative anomalies in  $\text{Cl}^-$  concentration may have alternative sources. The upward transport of chloride-depleted fluids from deep sediments may contribute to the anomalies. For example, at the Cascadia convergent continental margin, the temperatures at deep depths in the accretionary wedge sediments are higher than those in typical sediments. This elevated temperature may lead to the dehydration of smectite as it transforms into illite or the dehydration of opal. Due to compaction and diffusion, chloride-depleted freshwater from these deep sediments is transported upwards. Such phenomena, where clay minerals or opal dehydration produce chloride-depleted freshwater, can also be observed in the geological context of mud volcanoes [45,65–70]. Additionally, thick clay mineral layers exhibit a membrane filtration effect, resulting in the retention of  $\text{Cl}^-$ , D, and  $^{18}\text{O}$  in the pore water, while only freshwater is transported upwards [50]. However, membrane filtration leads to a depletion of D and  $^{18}\text{O}$ , which contrasts with the enrichment of D and  $^{18}\text{O}$  observed during hydrate dissociation [68].

### 3.2. $\delta^{18}\text{O}$ and $\delta\text{D}$ in Pore Water

During hydrate dissociation, the release of  $^{18}\text{O}$  and D from the hydrate water molecule cages into the pore water can be used to estimate hydrate saturation (Figure 4c,d) [43,71]. In practical studies, research on the independent quantification of saturation using pore water  $\delta\text{D}$  is limited [72]. This is due to the hydrogen isotope exchange between pore water

H<sub>2</sub>O and dissolved CH<sub>4</sub>, as well as the challenge of achieving high-precision measurements of δD [59]. Consequently, δD is more frequently employed as a qualitative proxy for identifying hydrates or as a reference value for saturation estimation with δ<sup>18</sup>O. The principles and methods for calculating hydrate saturation using δD and δ<sup>18</sup>O are fundamentally the same. This paper elaborates on the specific process of estimating hydrate saturation using the more widely applied δ<sup>18</sup>O values.



**Figure 4.** Schematic of temperature and corresponding infrared image (a), Cl<sup>−</sup> concentration (b), δD (c), δ<sup>18</sup>O (d), and the hydrate saturation (e) estimated from these parameters.

### 3.2.1. δ<sup>18</sup>O Values for Estimating Hydrate Saturation

The determination of δ<sup>18</sup>O in the hydrate zone and its pristine background value is analogous to the Cl<sup>−</sup> method (see Section 3.1). The estimated gas hydrate saturation value (S<sub>h</sub>) is first calculated via Equation (6) and subsequently substituted into Equation (4) [61]:

$$M = \frac{\delta^{18}O_h - \delta^{18}O_b}{\epsilon} \quad (6)$$

where δ<sup>18</sup>O<sub>h</sub> represents the δ<sup>18</sup>O of interstitial water collected from sediments in the gas hydrate zone, and δ<sup>18</sup>O<sub>b</sub> represents the baseline δ<sup>18</sup>O value. The enrichment factor ε quantifies the degree of enrichment of the <sup>18</sup>O isotope in the hydrate phase.

### 3.2.2. Factors Affecting the Estimation of Hydrate Saturation with δ<sup>18</sup>O

δ<sup>18</sup>O is one of the pore water proxies for estimating gas hydrate saturation. This method, similar to the Cl<sup>−</sup> method, is also subject to challenges related to insufficient diffusion. Moreover, some studies have observed an overall increase in δ<sup>18</sup>O values at depths below the gas hydrate stability zone in certain regions, despite no corresponding anomalies in the Cl<sup>−</sup> concentration profiles. Tomaru et al. attributed this phenomenon to the memory effect associated with hydrate formation and dissociation [59]. Experiments and molecular dynamics simulations have shown that gas hydrates tend to form in meltwater where gas hydrates had previously existed [73–76]. Researchers postulated that dissociated water from natural gas hydrates retains hydrogen bonds between oxygen atoms, remains enriched in <sup>18</sup>O and D, and provides a template for successive hydrate nucleation. The memory effect of hydrate formation and dissociation constrains only the participating water molecules (oxygen and hydrogen atoms) and does not affect Cl<sup>−</sup>. In study areas with a history of hydrate formation and dissociation, the overall increase in δ<sup>18</sup>O can complicate the determination of the baseline (δ<sup>18</sup>O<sub>b</sub>), potentially impacting the accuracy of saturation value estimation.

In addition to hydrate dissociation, the transport of fluids resulting from the dehydration of clay minerals in deep sediments can also contribute to an increase in δ<sup>18</sup>O values. The interlayer water of clay minerals is generally enriched in <sup>18</sup>O but depleted in D [77].



Consequently, the  $\delta D$  profile can help differentiate between the effects of clay mineral dehydration and hydrate dissociation. Furthermore, processes such as the residual  $^{18}O$ -enriched pore water from Quaternary glacial periods and the recrystallization of marine carbonates at temperatures higher than their initial formation temperature can also lead to elevated  $\delta^{18}O$  values. The extent of each process's contribution to the positive  $\delta^{18}O$  anomalies, in conjunction with  $\delta D$  profiles, can be used to identify the underlying causes [68,78].

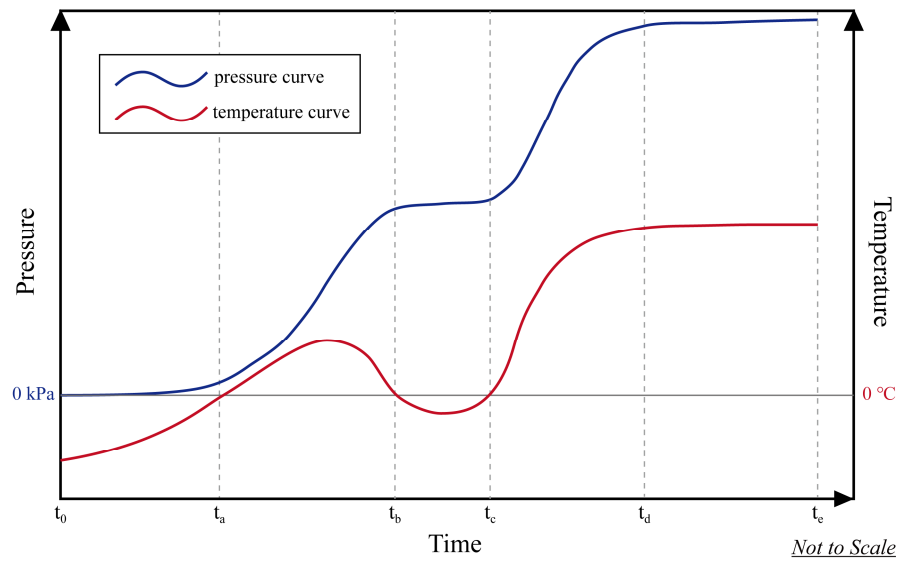
#### 4. Estimation of Hydrate Saturation Using Gas Released from Hydrate Dissociation

The principle of the gas volumetric method for estimating hydrate saturation involves collecting gas from core samples. The amount of gas, in conjunction with the hydration number  $n$  and hydrate density, is then utilized to calculate the volume of the hydrate. Once the pore volume is determined, the hydrate saturation can be obtained. This method yields a hydrate saturation value that remains unaffected by other physical, biological, or chemical processes in the marine environment and is regarded as the "gold standard" for saturation estimates [79,80]. However, the easily decomposable nature of gas hydrates presents significant challenges to their preservation [21]. Recent advancements in pressure core sampling technology have enabled the recovery of sediments under near in situ pressures, thereby minimizing hydrate dissociation during core retrieval [28,81,82].

Two primary approaches exist for estimating hydrate saturation using the gas volumetric method. The first approach involves calculating the quantity of gas in the hydrate by assessing the weight difference of the gas hydrate-bearing sediment before and after gas release. The second approach determines the volume of gas released from hydrate dissociation by measuring the pressure change in a fixed-volume vacuum chamber [21], a method that has been widely adopted by most studies.

Dissociation experiments on samples are conducted in a fixed-volume vacuum chamber, with the gas volume determined by the observed pressure increase [83]. Figure 5 presents a schematic representation of the pressure and temperature curves during hydrate dissociation, illustrating that hydrate dissociation is a multi-stage process. In the initial stage ( $t_0$  to  $t_a$ ), the hydrate is removed from liquid nitrogen, during which the hydrate begins dissociating very slowly at low temperatures. In stage  $t_a$  to  $t_b$ , the hydrate absorbs heat from the external environment and dissociates rapidly. Hydrate dissociation, being an endothermic process, causes a decrease in the surrounding environment's temperature. In stage  $t_b$  to  $t_c$ , as the system temperature drops below the freezing point, water freezes. The extremely low temperature and presence of ice hinder the endothermic dissociation of the hydrate, causing it to nearly cease. In stage  $t_c$  to  $t_d$ , as the system gains energy and the temperature rises; the ice melts, permitting the remaining hydrate to resume dissociation. Following stage  $t_d$ , the pressure curve reaches equilibrium, indicating the complete dissociation of the hydrates. The experiment should be terminated at stage  $t_e$ , at which point all hydrates have dissociated; otherwise, pore water in the sediment may evaporate, resulting in inaccurately high saturation values.

The hydration number of natural gas hydrates can be calculated using the integrated peak intensities of Raman or NMR spectra, along with gas composition [83]. Table 2 summarizes the hydration numbers ( $n$ ) of sI-type methane hydrates from various regions, typically ranging from 5.9 to 6.2. In studies where high precision is not required, the average hydration number  $n = 6$  is often used as the stoichiometric ratio for methane hydrates ( $CH_4 \cdot 6H_2O$ ) in subsequent calculations [19].



**Figure 5.** A schematic sketch of the pressure curve (blue) and temperature curve (red) of the hydrate dissociation experiment.  $t_0$  marks the beginning of the experiment;  $t_a$ ,  $t_b$ ,  $t_c$ , and  $t_d$  denote key time points in the experimental process; and  $t_e$  indicates the end of the experiment.

**Table 2.** Hydration number  $n$  of sl-type methane hydrates worldwide.

Sample Location	Hydration Number $n$ (sl-Type)	Reference
Blake Ridge (off South Carolina)	6.2	[84]
Hydrate Ridge (off Oregon)	6.11	[85]
Eastern Nankai Trough, Japan	6.1–6.2	[86]
Mallik, Canada	6.1–6.3	[87]
offshore Vancouver Island, Canada	6.1	[88]
Northern Cascadia margin, Canada	6.1–6.5	[89]
Elbert, Canada	6.1	[83]
Lake Baikal, Russia	6.1–6.2	[90]
Shenhu area, South China Sea	5.9	[91]
Qiongdongnan Basin, South China Sea	6.12–6.19	[92]
K-G Basin, India	6.1–6.2	[93]

The pore volume of sediments is typically approximated by the volume of pore water, assuming that pore water fully occupies the pore space within the sediments. The pore volume can be calculated by combining the density of the pore water with the mass difference of the sediments before and after drying (i.e., the mass of the water). Alternative methods, such as specimen mass calculations, logging-while-drilling data, or NMR tool measurements, can also be used to determine pore volume [94].

The volume of methane released from degassing needs to be subtracted from the solubility of methane, and the remainder is assumed to be present in the methane hydrate phase. The corresponding formulae are as follows [19]:

$$n_{GH-CH_4} = n_{total\ gas} - n_{dissolved} = \frac{V_{total\ gas}}{V_m} - V_{pore} \cdot c_{CH_4} \approx \frac{V_{total\ gas}}{V_m} \quad (7)$$

$$m_{GH} = n_{GH-CH_4} \cdot M_{CH_4 \cdot nH_2O} \quad (8)$$

$$V_{GH} = \frac{m_{GH}}{\rho_{GH}} \quad (9)$$

$$S_{GH} = \frac{V_{GH}}{V_{pore}} \quad (10)$$

Equation (7) represents the moles of methane in the natural gas hydrate after accounting for the dissolved methane. The total moles of methane gas ( $n_{total\ gas}$ ) are calculated from the collected total methane gas volume ( $V_{total\ gas}$ ) and the molar volume of gas ( $V_m = 22.4\ L/mol$  at  $0\ ^\circ C$ ). The moles of dissolved methane ( $n_{dissolved}$ ) can be determined from the saturation solubility of methane ( $c_{CH_4}$ ) and the pore volume ( $V_{pore}$ ). However, solubility data from Handa (1990) suggest that the gas/water ratio for a methane-saturated solution under shallow geological conditions (e.g., in sediments at temperatures below  $30\ ^\circ C$  and pressures below 30 MPa) is less than 0.05, which is negligible compared to the nominal gas/water ratio of methane hydrate ( $\sim 160$ ) [95]. Thus, it is reasonable to assume that all the gas recovered from gas hydrate dissociation originated from gas hydrate, i.e.,  $n_{GH-CH_4} \approx n_{total\ gas}$ .

Once the hydration number  $n$  is determined, the molar mass of the hydrate ( $M_{CH_4 \cdot nH_2O}$ ) can be established, allowing the mass of the hydrate ( $m_{GH}$ ) to be calculated, as shown in Equation (8) [28]. Subsequently, using the density of the gas hydrate ( $\rho_{GH} \approx 0.92\ g \cdot cm^{-3}$ ), the volume of the hydrate can be determined, as shown in Equation (9) [83]. The density of methane hydrate varies depending on its structure and can be derived through XRD refinement. In the final step, the natural gas hydrate saturation ( $S_{GH}$ ) is determined using Equation (10).

Errors in estimating natural gas hydrate saturation using the gas volumetric method stem from inaccuracies in determining both the hydrate volume and the pore volume. The volume of natural gas hydrates may have partially dissociated prior to laboratory dissociation and degassing, even when using pressure-core sampling techniques [79]. Some sampling procedures involve storing experimental sediment samples in a methane gas-pressurized environment to inhibit dissociation; however, this can lead to the formation of new hydrates, resulting in an overestimation of the measured saturation [83,96].

The error in pore volume estimation primarily arises from the assumption that the pore volume is approximately equivalent to the pore water volume. The density of pore water differs from that of hydrate, leading to an error when directly equating the calculated pore water volume to the actual pore volume. This error can be corrected using the dimensionless constant  $\beta$  mentioned in Section 3.1. Another significant source of error in pore volume estimation is the presence of free gas. Free gas occupies a portion of the pores, resulting in the actual pore water volume being less than the total pore volume. This discrepancy leads to an underestimation of the pore volume and an overestimation of hydrate saturation.

## 5. Estimation of Hydrate Saturation with Core Temperature Anomaly

During core recovery, gas hydrate rapidly dissociates as the temperature and pressure conditions are outside the stable regime for gas hydrate. Since this dissociation is an endothermic process, hydrate-containing zones cool relative to the surrounding sediments, resulting in negative temperature anomalies [97]. An infrared camera can be used to image the entire sample and identify localized cold zones in the core, as shown in the infrared image (Figure 4a) [97,98]. Infrared images from a specific location showing a cooling trend over time indicate ongoing gas hydrate dissociation, necessitating prompt sampling. Conversely, a warming trend suggests that the gas hydrate has fully dissociated. The position, dissociation state, and quantity of hydrate can be qualitatively assessed by analyzing temperature anomalies [5,61].

Given the high sampling resolution of infrared scanning data (up to 2 cm), some studies have employed infrared data to quantitatively estimate hydrate saturation [98]. This method necessitates the calibration of the relationship between temperature anomalies ( $\Delta T$ ) and hydrate content, such as through a "threshold" function. However, these conversion functions are often imprecise, with varying values observed at different measurement times, and their application across different regions is challenging [12]. Additionally, other

sources of uncertainty in infrared-based estimates of gas hydrate content include incomplete core recovery, the misidentification of anomalies not caused by natural gas hydrates (e.g., dissolved gas degassing leading to negative temperature anomalies), and the possibility that not all hydrates produce recognizable anomalies, etc. Although the quantitative calculation of hydrate saturation from infrared-derived negative temperature anomalies lacks precision, it can be integrated with other methods to derive saturation values. For example, a strong correlation exists between the  $Cl^-$  concentration in hydrate-bearing layers and the temperature anomalies [12], and the  $\Delta T - \Delta Cl^-$  combination method can effectively determine the saturation and distribution of hydrate [39]. In practical applications, infrared data is more commonly utilized for the rapid detection of gas hydrate buried by sediments and for the preliminary, non-precise estimation of hydrate quantities due to its non-destructive and rapid characteristics, thereby providing a reference for subsequent detailed hydrate analysis.

## 6. Discussion

### 6.1. Comparison of Different Methods

Hydrate saturation values derived from core sediments are commonly regarded as reliable estimates, with their associated strengths and limitations outlined in Table 3.

**Table 3.** Comparison of methods for determining hydrate saturation in marine sediments.

	Gas Volumetric Method	Chloride Concentration Method	Isotopic Method ( $\delta^{18}O/\delta D$ )	Infrared Temperature Anomaly Method
Application condition	No dissociation of hydrates after core recovery; gas released is collected under control	Determines $Cl^-$ concentration following hydrate dissociation	Determines the isotopic values of pore water following hydrate dissociation	Infrared scanning after core recovery
Core Quality Requirements	High quality cores; preserves in situ conditions	Less stringent; tolerates minor dissociation	\	\
Non-Destructive Measurements	Allows Xray, P-wave, and gamma density measurements	\	\	Non-destructive measurements
Accuracy	Considers the ground-truth value	Reliable with minor dissociation when recovered	Similar to $Cl^-$ but challenging to measure	Provides qualitative estimates
Cost	High cost	\	\	\
Challenges	Requires pressure/temperature maintenance	Requires careful determination of the calculation parameters	Logistical difficulty especially for onboard isotopic measurement	Subject to numerous interfering factors
Applicability	Used in both laboratory and field settings	Widely used onboard	Less frequent due to measurement challenges	Widely used for qualitative field assessments

Hydrate saturation obtained via the gas volumetric method is widely considered to represent the ground-truth value. This method requires maintaining in situ pressure and temperature through pressure cores during core sampling, which preserves hydrates in conditions close to their natural state and mitigates dissociation. Pressure cores not only facilitate the calculation of saturation but also enable the study of hydrate morphology, type, and the in situ physical properties of the host sediments. Non-destructive measurements such as X-ray imaging, P-wave velocity, and gamma density can also be conducted during pressure maintenance and dissociation processes to investigate the behavior of gas hydrates within the sediments and to archive gas hydrate-bearing sediments under in situ pressures for future field investigations [19]. Theoretically, it is feasible to analyze chloride ions and the isotopic composition of oxygen and hydrogen in the pore water following hydrate dissociation in pressure cores to yield corresponding saturation values. Furthermore, since the gas volumetric method directly measures the amount of gas released during hydrate dissociation, it offers broader applicability compared to other methods. In laboratory experiments on hydrate formation and dissociation, such as investigations on

the dissociation driving force of methane hydrate in porous media and the dissociation of methane hydrate by hot brine, hydrate content is typically measured using the gas volumetric method [99–104]. Despite these advantages, the gas volumetric method has stringent application conditions; even minor hydrate dissociation can compromise its accuracy, and maintaining pressure and temperature during core sampling is challenging and costly.

The chlorinity anomaly method is perhaps the most widely used approach for determining hydrate saturation in marine sediments during field experiments, especially in cases where pressure core sampling techniques have not yet been developed or where economic constraints are a concern [27,45,105]. The  $\text{Cl}^-$  method also imposes less stringent sediment quality requirements compared to the gas volumetric method. In cases of minor hydrate dissociation, if the freshening effects resulting from hydrate dissociation remain preserved in the sediment's pore water, then a small degree of hydrate dissociation in the recovered cores does not substantially affect the estimation of hydrate saturation. The principle behind the  $\delta^{18}\text{O}$  or  $\delta\text{D}$  method for estimating saturation is similar to that of the  $\text{Cl}^-$  method. However, due to the challenges of measuring isotopic values onboard, chloride concentration can be more easily determined through ion chromatography or molar titration, making this method significantly more prevalent than isotopic measurements.

The quantitative application of the infrared temperature anomaly method is constrained by factors such as the mechanical and thermal characteristics of coring tools, recovery rates, temperature gradients in the water column, gas hydrate morphology, and the thermal properties of the primary sediment. Nevertheless, it is widely employed for determining hydrate depth and qualitative estimations. Before conducting chloride analysis or gas volumetric analysis, infrared imaging is used to identify the background trends of hydrate presence.

## 6.2. Limitations and Gaps

The sources of error in estimating hydrate saturation in core samples can be summarized as follows: the inability to obtain entirely accurate values (e.g.,  $\text{Cl}^-$  concentrations are influenced by diffusion and other marine processes, or dissociation prior to gas collection and the mixing of free gas in the gas volume method), and uncertainties in parameter determination during calculations (e.g., hydrate density, pore water density, hydration number  $n$ ).

The heterogeneous and irregular distribution of hydrates affects the representativeness of saturation values at the reservoir scale. In sandy sediments with large pore spaces and high permeability (e.g., turbidite systems in fluvial environments [106], the Gulf of Mexico [107], and the Nankai Trough [108]), hydrates typically exist in pore-filling forms. In certain silty sediments such as the Blake Plateau [109], the Shenhu area in the South China Sea [110], and the Gulf of Mexico [111], due to the presence of abundant foraminifera shells, diatoms, and pyrite, which typically have high porosity and permeability, hydrates are filled within biological shells. In muddy silty sediments with small particle pores, it is challenging for hydrates to fill fine-grained sediment pores, and they likely occupy fractures of varying shapes and sizes. As emphasized in Section 1, the definition of saturation primarily applies to pore-filling hydrates; however, in reality, hydrates in reservoirs often coexist in both pore-filling and fracture-filling forms [112]. Estimating hydrate abundance in zones dominated by fracture-type distributions remains particularly challenging.

Current methods for estimating hydrate saturation predominantly focus on methane hydrates. However, hydrate gases may originate from mixed sources containing methane, ethane, or other gases, leading to different hydration numbers and corresponding densities, thus requiring gas composition measurements for accurate saturation calculations.

## 7. Conclusions and Prospectives

The saturation of natural gas hydrates is a critical parameter for quantifying the resource potential of pore-filling hydrates uniformly distributed within sediments. Several methods have been developed to estimate gas hydrate saturation, among which the pore



water chemistry-based method, the gas volumetric method, and the temperature anomaly-based method are widely employed for estimating hydrate saturation in sediments.

- The pore water chemistry-based methods estimate hydrate saturation by analyzing the negative anomaly in chlorinity caused by the freshening process and the positive anomaly in  $\delta^{18}\text{O}$  or  $\delta\text{D}$  values resulting from the mixture of heavy isotopes in the hydrate phase. These methods should be applied after hydrate dissociation, with careful consideration given to potential seawater contamination and interference from other geological processes.
- The gas volumetric method provides a relatively direct estimation of hydrate saturation, applicable to well-preserved, intact core samples where hydrate has not dissociated prior to degassing experiments.
- The temperature anomaly-based method infers the distribution of hydrate and estimates saturation based on the negative temperature anomaly resulting from endothermic hydrate dissociation. Infrared temperature anomalies are good indicators for locating hydrates buried by sediments and offer a preliminary understanding of the amount of hydrate, though the precision in quantitative saturation estimation is limited.

To evaluate hydrate resources with greater accuracy and cost-efficiency, future improvements in estimating hydrate saturation should proceed in the following directions:

- As various types of hydrates continue to be discovered, methods for estimating the saturation of hydrates from different gas sources or structure types should be developed and refined.
- To more economically assess the resource potential of large-scale hydrate reservoirs, the results of infrared temperature anomaly, pore water proxies, gas volumetric analysis, and geophysical resistivity and seismic methods should be integrated. Furthermore, a comprehensive application of the results from several methods can be incorporated into numerical simulations or rock geophysical models to evaluate the hydrate resource.

**Author Contributions:** Conceptualization, H.L.; writing—original draft preparation, Y.X.; writing—review and editing, Y.X., H.L., W.C., H.Y. and L.Z.; visualization, Y.X. and H.L.; supervision, H.L.; project administration, H.L. All authors have read and agreed to the published version of the manuscript.

**Funding:** This research was funded by DD20221703, DD20230063 from the China Geological Survey and The Guangdong Major project of Basic and Applied Basic Research (No. 2020B0301030003).

**Conflicts of Interest:** The authors declare no conflicts of interest.

## References

1. Sloan, E.D. Fundamental Principles and Applications of Natural Gas Hydrates. *Nature* **2003**, *426*, 353–359. [[CrossRef](#)]
2. Uchida, T.; Dallimore, S.; Mikami, J. Occurrences of Natural Gas Hydrates beneath the Permafrost Zone in Mackenzie Delta: Visual and X-Ray CT Imagery. *Ann. N. Y. Acad. Sci.* **2000**, *912*, 1021–1033. [[CrossRef](#)]
3. Makogon, Y.F. Natural Gas Hydrates—A Promising Source of Energy. *J. Nat. Gas Sci. Eng.* **2010**, *2*, 49–59. [[CrossRef](#)]
4. Chong, Z.R.; Yang, S.H.B.; Babu, P.; Linga, P.; Li, X.-S. Review of Natural Gas Hydrates as an Energy Resource: Prospects and Challenges. *Appl. Energy* **2016**, *162*, 1633–1652. [[CrossRef](#)]
5. Wei, J.; Liang, J.; Lu, J.; Zhang, W.; He, Y. Characteristics and Dynamics of Gas Hydrate Systems in the Northwestern South China Sea—Results of the Fifth Gas Hydrate Drilling Expedition. *Mar. Pet. Geol.* **2019**, *110*, 287–298. [[CrossRef](#)]
6. Ghosh, R.; Ojha, M.; Kumar, P. Review of Rock Physics Theories for Quantifying Gas Hydrate and Associated Uncertainties. *J. Asian Earth Sci.* **2023**, *256*, 105828. [[CrossRef](#)]
7. Ding, Y.; Qian, A.; Lu, H. Influences of Hydrate Morphology and Hydrate Distribution Heterogeneity on the Mechanical Properties of Hydrate-Bearing Sediments Using the Discrete Element Method. *Geomech. Geophys. Geo-Energ. Geo-Resour.* **2022**, *8*, 106. [[CrossRef](#)]
8. Soga, K.; Ng, M.; Lee, S.; Klar, A. Characterisation and Engineering Properties of Methane Hydrate Soils. In *Characterisation and Engineering Properties of Natural Soils*; Phoon, K., Hight, D., Leroueil, S., Tan, T., Eds.; Taylor & Francis: Abingdon-on-Thames, UK, 2007; Volume 3–4, pp. 2591–2642. ISBN 978-0-415-42691-6.
9. Boswell, R.; Yamamoto, K.; Lee, S.-R.; Collett, T.; Kumar, P.; Dallimore, S. Chapter 8—Methane Hydrates. In *Future Energy*, 2nd ed.; Letcher, T.M., Ed.; Elsevier: Boston, MA, USA, 2014; pp. 159–178. ISBN 978-0-08-099424-6.
10. Xie, Y.; Li, R.; Wang, X.-H.; Zheng, T.; Cui, J.-L.; Yuan, Q.; Qin, H.-B.; Sun, C.-Y.; Chen, G.-J. Review on the Accumulation Behavior of Natural Gas Hydrates in Porous Sediments. *J. Nat. Gas Sci. Eng.* **2020**, *83*, 103520. [[CrossRef](#)]



11. Guo, W.; Li, Y.; Jia, R.; Wang, Y.; Tang, G.; Li, X. Experimental Study on Mechanical Properties of Pore-Filling and Fracture-Filling Clayey Silt Hydrate-Bearing Sediments. *Energy* **2023**, *284*, 129354. [[CrossRef](#)]
12. Tréhu, A.M.; Long, P.E.; Torres, M.E.; Bohrmann, G.; Rack, F.R.; Collett, T.S.; Goldberg, D.S.; Milkov, A.V.; Riedel, M.; Schultheiss, P.; et al. Three-Dimensional Distribution of Gas Hydrate beneath Southern Hydrate Ridge: Constraints from ODP Leg 204. *Earth Planet. Sci. Lett.* **2004**, *222*, 845–862. [[CrossRef](#)]
13. Milkov, A.V.; Dickens, G.R.; Claypool, G.E.; Lee, Y.-J.; Borowski, W.S.; Torres, M.E.; Xu, W.; Tomaru, H.; Tréhu, A.M.; Schultheiss, P. Co-Existence of Gas Hydrate, Free Gas, and Brine within the Regional Gas Hydrate Stability Zone at Hydrate Ridge (Oregon Margin): Evidence from Prolonged Degassing of a Pressurized Core. *Earth Planet. Sci. Lett.* **2004**, *222*, 829–843. [[CrossRef](#)]
14. Qin, X.; Lu, J.; Lu, H.; Qiu, H.; Liang, J.; Kang, D.; Zhan, L.; Lu, H.; Kuang, Z. Coexistence of Natural Gas Hydrate, Free Gas and Water in the Gas Hydrate System in the Shenhu Area, South China Sea. *China Geol.* **2020**, *3*, 210–220. [[CrossRef](#)]
15. Ecker, C.; Dvorkin, J.; Nur, A.M. Estimating the Amount of Gas Hydrate and Free Gas from Marine Seismic Data. In *Methods and Applications in Reservoir Geophysics*; Johnston, D.H., Abriél, W.L., Ahmad, F.I., Brown, A.R., Jack, I.G., Lewallen, K.T., MacBeth, C.D., Muhuri, S.K., Payne, M.A., Schuelke, J.S., et al., Eds.; Society of Exploration Geophysicists: Houston, TX, USA, 2010; Volume 15, ISBN 978-1-56080-216-7.
16. Guo, K.; Fan, S.; Wang, Y.; Lang, X.; Zhang, W.; Li, Y. Physical and Chemical Characteristics Analysis of Hydrate Samples from Northern South China Sea. *J. Nat. Gas Sci. Eng.* **2020**, *81*, 103476. [[CrossRef](#)]
17. Colwell, F.; Matsumoto, R.; Reed, D. A Review of the Gas Hydrates, Geology, and Biology of the Nankai Trough. *Chem. Geol.* **2004**, *205*, 391–404. [[CrossRef](#)]
18. Matsumoto, R. Methane Hydrate Estimates from the Chloride and Oxygen Isotopic Anomalies: Examples from the Blake Ridge and Nankai Trough Sediments. *Ann. N. Y. Acad. Sci.* **2000**, *912*, 39–50. [[CrossRef](#)]
19. Lee, J.Y.; Jung, J.W.; Lee, M.H.; Bahk, J.-J.; Choi, J.; Ryu, B.-J.; Schultheiss, P. Pressure Core Based Study of Gas Hydrates in the Ulleung Basin and Implication for Geomechanical Controls on Gas Hydrate Occurrence. *Mar. Pet. Geol.* **2013**, *47*, 85–98. [[CrossRef](#)]
20. Lee, M.W.; Collett, T.S. In-Situ Gas Hydrate Saturation Estimated from Various Well Logs at the Mount Elbert Gas Hydrate Stratigraphic Test Well, Alaska North Slope. *Mar. Pet. Geol.* **2011**, *28*, 439–449. [[CrossRef](#)]
21. Lu, H.; Dutrisac, D.; Ripmeester, J.; Wright, F.; Uchida, T. *Measurements of Gas Hydrate Saturation in Sediment Cores Recovered from the JAPEX/JNOC/GSC et al. Mallik 5L-38 Gas Hydrate Production Research Well*; Scientific Results from the Mallik 2002 Gas Hydrate Production Research Well Program, Mackenzie Delta, Northwest Territories, Canada; Geological Survey of Canada: Vancouver, BC, Canada, 2005.
22. Holland, M.E.; Schultheiss, P.J.; Roberts, J.A. Gas Hydrate Saturation and Morphology from Analysis of Pressure Cores Acquired in the Bay of Bengal during Expedition NGHP-02, Offshore India. *Mar. Pet. Geol.* **2019**, *108*, 407–423. [[CrossRef](#)]
23. Heeschen, K.U.; Haeckel, M.; Klaucke, I.; Ivanov, M.K.; Bohrmann, G. Quantifying In-Situ Gas Hydrates at Active Seep Sites in the Eastern Black Sea Using Pressure Coring Technique. *Biogeosciences* **2011**, *8*, 3555–3565. [[CrossRef](#)]
24. Zhang, G.; Liang, J.; Lu, J.; Yang, S.; Zhang, M.; Holland, M.; Schultheiss, P.; Su, X.; Sha, Z.; Xu, H.; et al. Geological Features, Controlling Factors and Potential Prospects of the Gas Hydrate Occurrence in the East Part of the Pearl River Mouth Basin, South China Sea. *Mar. Pet. Geol.* **2015**, *67*, 356–367. [[CrossRef](#)]
25. Dickens, G.R.; Wallace, P.J.; Paull, C.K.; Borowski, W.S. Detection of Methane Gas Hydrate in the Pressure Core Sampler (PCS): Volume-Pressure-Time Relations during Controlled Degassing Experiments. *Proc. Ocean. Drill. Program Sci. Results* **2000**, *164*, 113–126.
26. Haines, S.S.; Collett, T.S.; Yoneda, J.; Shimoda, N.; Boswell, R.; Okinaka, N. Gas Hydrate Saturation Estimates, Gas Hydrate Occurrence, and Reservoir Characteristics Based on Well Log Data from the Hydrate-01 Stratigraphic Test Well, Alaska North Slope. *Energy Fuels* **2022**, *36*, 3040–3050. [[CrossRef](#)]
27. Wang, X.; Wu, S.; Lee, M.; Guo, Y.; Yang, S.; Liang, J. Gas Hydrate Saturation from Acoustic Impedance and Resistivity Logs in the Shenhu Area, South China Sea. *Mar. Pet. Geol.* **2011**, *28*, 1625–1633. [[CrossRef](#)]
28. Dickens, G.R.; Paull, C.K.; Wallace, P. Direct Measurement of In Situ Methane Quantities in a Large Gas-Hydrate Reservoir. *Nature* **1997**, *385*, 426–428. [[CrossRef](#)]
29. Zhan, L.; Kang, D.; Lu, H.; Lu, J. Characterization of Coexistence of Gas Hydrate and Free Gas Using Sonic Logging Data in the Shenhu Area, South China Sea. *J. Nat. Gas Sci. Eng.* **2022**, *101*, 104540. [[CrossRef](#)]
30. Zhan, L.; Liu, B.; Zhang, Y.; Lu, H. Rock Physics Modeling of Acoustic Properties in Gas Hydrate-Bearing Sediment. *J. Mar. Sci. Eng.* **2022**, *10*, 1076. [[CrossRef](#)]
31. Kang, D.; Xie, Y.; Lu, J.; Wang, T.; Liang, J.; Lai, H.; Fang, Y. Assessment of Natural Gas Hydrate Reservoirs at Site GMGS3-W19 in the Shenhu Area, South China Sea Based on Various Well Logs. *China Geol.* **2022**, *5*, 383–392. [[CrossRef](#)]
32. Davidson, D.W.; Leaist, D.G.; Hesse, R. Oxygen-18 Enrichment in the Water of a Clathrate Hydrate. *Geochim. Cosmochim. Acta* **1983**, *47*, 2293–2295. [[CrossRef](#)]
33. Cai, Z.; Lu, H.; Zou, R.; Han, S.; Wang, Z. Structural and Thermodynamic Characteristics of sH 2,2-Dimethylbutane-Methane Deuterohydrate. *J. Chem. Thermodyn.* **2014**, *77*, 82–86. [[CrossRef](#)]
34. Nagano, Y.; Miyazaki, Y.; Matsuo, T.; Suga, H. Heat Capacities and Enthalpy of Fusion of Heavy Oxygen Water. *J. Phys. Chem.* **1993**, *97*, 6897–6901. [[CrossRef](#)]

35. Seo, Y.; Lee, H.; Ryu, B.-J. Hydration Number and Two-Phase Equilibria of CH<sub>4</sub> Hydrate in the Deep Ocean Sediments. *Geophys. Res. Lett.* **2002**, *29*, 85-1–85-4. [[CrossRef](#)]
36. Sloan, E.D.; Koh, C.A. *Clathrate Hydrates of Natural Gases*, 3rd ed.; CRC Press: Boca Raton, FL, USA, 2007; ISBN 978-0-429-12914-8.
37. Sloan, E.D. Physical/Chemical Properties of Gas Hydrates and Application to World Margin Stability and Climatic Change. *Geol. Soc. Lond. Spec. Publ.* **1998**, *137*, 31–50. [[CrossRef](#)]
38. Guan, W.; Cai, W.; Li, Z.; Lu, H. Microscopic Characterization and Fractal Analysis of Pore Systems for Unconventional Reservoirs. *J. Mar. Sci. Eng.* **2024**, *12*, 908. [[CrossRef](#)]
39. Bohrmann, G.; Torres, M. Gas Hydrates in Marine Sediments. In *Marine Geochemistry*; Springer: Berlin/Heidelberg, Germany, 2006; pp. 481–512. ISBN 978-3-540-32143-9.
40. Rogner, H.-H.; Aguilera, R.; Archer, C.; Bertani, R.; Bhattacharya, S.; Dusseault, M.; Gagnon, L.; Haberl, H.; Hoogwijk, M.; Johnson, A.; et al. Chapter 7—Energy Resources and Potentials. In *Global Energy Assessment—Toward a Sustainable Future*; Cambridge University Press: Cambridge, UK, 2012; pp. 423–512.
41. You, K.; Flemings, P.B.; Malinverno, A.; Collett, T.S.; Darnell, K. Mechanisms of Methane Hydrate Formation in Geological Systems. *Rev. Geophys.* **2019**, *57*, 1146–1196. [[CrossRef](#)]
42. Sun, S.; Zhao, J.; Yu, D. Dissociation Enthalpy of Methane Hydrate in Salt Solution. *Fluid Phase Equilibria* **2018**, *456*, 92–97. [[CrossRef](#)]
43. Hesse, R.; Harrison, W.E. Gas Hydrates (Clathrates) Causing Pore-Water Freshening and Oxygen Isotope Fractionation in Deep-Water Sedimentary Sections of Terrigenous Continental Margins. *Earth Planet. Sci. Lett.* **1981**, *55*, 453–462. [[CrossRef](#)]
44. Ussler, W.; Paull, C.K. Effects of Ion Exclusion and Isotopic Fractionation on Pore Water Geochemistry during Gas Hydrate Formation and Decomposition. *Geo-Mar. Lett.* **1995**, *15*, 37–44. [[CrossRef](#)]
45. Ussler III, W.; Paull, C.K. Ion Exclusion Associated with Marine Gas Hydrate Deposits. In *Natural Gas Hydrates: Occurrence, Distribution, and Detection*; Geophysical Monograph Series; American Geophysical Union: Washington, DC, USA, 2001; pp. 41–51. ISBN 978-1-118-66841-2.
46. Haekel, M.; Suess, E.; Wallmann, K.; Rickert, D. Rising Methane Gas Bubbles Form Massive Hydrate Layers at the Seafloor. *Geochim. Cosmochim. Acta* **2004**, *68*, 4335–4345. [[CrossRef](#)]
47. Malinverno, A.; Kastner, M.; Torres, M.E.; Wortmann, U.G. Gas Hydrate Occurrence from Pore Water Chlorinity and Downhole Logs in a Transect across the Northern Cascadia Margin (Integrated Ocean Drilling Program Expedition 311). *J. Geophys. Res. Solid Earth* **2008**, *113*, B08103. [[CrossRef](#)]
48. Maekawa, T.; Imai, N. Hydrogen and Oxygen Isotope Fractionation in Water during Gas Hydrate Formation. *Ann. N. Y. Acad. Sci.* **2000**, *912*, 452–459. [[CrossRef](#)]
49. Kastner, M.; Kvenvolden, K.A.; Lorenson, T.D. Chemistry, Isotopic Composition, and Origin of a Methane-Hydrogen Sulfide Hydrate at the Cascadia Subduction Zone. *Earth Planet. Sci. Lett.* **1998**, *156*, 173–183. [[CrossRef](#)]
50. Tomaru, H.; Torres, M.E.; Matsumoto, R.; Borowski, W.S. Effect of Massive Gas Hydrate Formation on the Water Isotopic Fractionation of the Gas Hydrate System at Hydrate Ridge, Cascadia Margin, Offshore Oregon. *Geochem. Geophys. Geosyst.* **2006**, *7*, Q10001. [[CrossRef](#)]
51. Maekawa, T. Experimental Study on Isotopic Fractionation in Water during Gas Hydrate Formation. *Geochem. J.* **2004**, *38*, 129–138. [[CrossRef](#)]
52. Matsumoto, R.; Borowski, W.S. Gas Hydrate Estimates from Newly Determined Oxygen Isotopic Fractionation ( $\alpha(\text{GH-IW})$ ) and  $\delta^{18}\text{O}$  Anomalies of the Interstitial Waters: Leg 164, Blake Ridge. *Proc. Ocean. Drill. Program Sci. Results* **2000**, *164*, 59–66.
53. Kvenvolden, K.A.; Kastner, M. Gas Hydrates of the Peruvian Outer Continental Margin. *Proc. Ocean. Drill. Program Sci. Results* **1990**, *112*, 517–526.
54. Handa, Y.P. Enthalpies of fusion and heat capacities for H<sub>2</sub><sup>18</sup>O ice and H<sub>2</sub><sup>18</sup>O tetrahydrofuran clathrate hydrate in the range 100–270 K. *Can. J. Chem.* **1984**, *62*, 1659–1661. [[CrossRef](#)]
55. Jakli, G.; Staschewski, D. Vapour Pressure of H<sub>2</sub><sup>18</sup>O Ice (–50 to 0 °C) and H<sub>2</sub><sup>18</sup>O Water (0 to 170 °C). *J. Chem. Soc. Faraday Trans. 1 Phys. Chem. Condens. Phases* **1977**, *73*, 1505–1509. [[CrossRef](#)]
56. Suzuoki, T.; Kimura, T. D/H and 18O/16O Fractionation in Ice-Water System. *J. Mass Spectrom. Soc. Jpn.* **1973**, *21*, 229–233. [[CrossRef](#)]
57. O’Neil, J.R. Hydrogen and Oxygen Isotope Fractionation between Ice and Water. *J. Phys. Chem.* **1968**, *72*, 3683–3684. [[CrossRef](#)]
58. Craig, H.; Hom, B. Relationships of D, 18O and Chlorinity in the Formation of Sea Ice. *Trans. Am. Geophys. Union* **1968**, *49*, 216–217.
59. Tomaru, H.; Matsumoto, R.; Lu, H.; Uchida, T. Geochemical Process of Gas Hydrate Formation in the Nankai Trough Based on Chloride and Isotopic Anomalies in Interstitial Water. *Resour. Geol.* **2004**, *54*, 45–51. [[CrossRef](#)]
60. Torres, M.E.; Collett, T.S.; Rose, K.K.; Sample, J.C.; Agena, W.F.; Rosenbaum, E.J. Pore Fluid Geochemistry from the Mount Elbert Gas Hydrate Stratigraphic Test Well, Alaska North Slope. *Mar. Pet. Geol.* **2011**, *28*, 332–342. [[CrossRef](#)]
61. Torres, M.E.; Tréhu, A.M.; Cespedes, N.; Kastner, M.; Wortmann, U.G.; Kim, J.-H.; Long, P.; Malinverno, A.; Pohlman, J.W.; Riedel, M.; et al. Methane Hydrate Formation in Turbidite Sediments of Northern Cascadia, IODP Expedition 311. *Earth Planet. Sci. Lett.* **2008**, *271*, 170–180. [[CrossRef](#)]

62. Reitz, A.; Pape, T.; Haeckel, M.; Schmidt, M.; Berner, U.; Scholz, F.; Liebetrau, V.; Aloisi, G.; Weise, S.M.; Wallmann, K. Sources of Fluids and Gases Expelled at Cold Seeps Offshore Georgia, Eastern Black Sea. *Geochim. Cosmochim. Acta* **2011**, *75*, 3250–3268. [[CrossRef](#)]
63. Makogon, Y.F. *Hydrates of Hydrocarbons*; PennWell Books: Tulsa, OK, USA, 1997.
64. Ye, J.; Wei, J.; Liang, J.; Lu, J.; Lu, H.; Zhang, W. Complex Gas Hydrate System in a Gas Chimney, South China Sea. *Mar. Pet. Geol.* **2019**, *104*, 29–39. [[CrossRef](#)]
65. Ross, D.A.; Degens, E.T. Recent Sediments of Black Sea<sup>1</sup>. In *The Black Sea—Geology, Chemistry, and Biology*; American Association of Petroleum Geologists: Tulsa, OK, USA, 1974; ISBN 978-1-62981-215-1.
66. Gieskes, J.; Blanc, G.; Vrolijk, P.; Elderfield, H.; Barnes, R. Interstitial Water Chemistry—Major Constituents. *Proc. Ocean. Drill. Program Sci. Results* **1990**, *110*, 155–178.
67. Kastner, M.; Elderfield, H.; Martin, J.B.; Tarney, J.; Pickering, K.T.; Knipe, R.J.; Dewey, J.F. Fluids in Convergent Margins: What Do We Know about Their Composition, Origin, Role in Diagenesis and Importance for Oceanic Chemical Fluxes? *Philos. Trans. R. Soc. Lond. Ser. A Phys. Eng. Sci.* **1997**, *335*, 243–259. [[CrossRef](#)]
68. Dählmann, A.; de Lange, G.J. Fluid–Sediment Interactions at Eastern Mediterranean Mud Volcanoes: A Stable Isotope Study from ODP Leg 160. *Earth Planet. Sci. Lett.* **2003**, *212*, 377–391. [[CrossRef](#)]
69. Torres, M.E.; Teichert, B.M.A.; Tréhu, A.M.; Borowski, W.; Tomaru, H. Relationship of Pore Water Freshening to Accretionary Processes in the Cascadia Margin: Fluid Sources and Gas Hydrate Abundance. *Geophys. Res. Lett.* **2004**, *31*, L22305. [[CrossRef](#)]
70. Kim, J.-H.; Park, M.-H.; Chun, J.-H.; Lee, J.Y. Molecular and Isotopic Signatures in Sediments and Gas Hydrate of the Central/Southwestern Ulleung Basin: High Alkalinity Escape Fuelled by Biogenically Sourced Methane. *Geo-Mar. Lett.* **2011**, *31*, 37–49. [[CrossRef](#)]
71. Hesse, R.; Frape, S.K.; Egeberg, P.K.; Matsumoto, R. Stable Isotope Studies (Cl, O, and H) of Interstitial Waters from Site 997, Blake Ridge Gas Hydrate Field, West Atlantic. *Proc. Ocean. Drill. Program Sci. Results* **2000**, *164*, 129–137. [[CrossRef](#)]
72. Hesse, R. Pore Water Anomalies of Submarine Gas-Hydrate Zones as Tool to Assess Hydrate Abundance and Distribution in the Subsurface What Have We Learned in the Past Decade? *Earth-Sci. Rev.* **2003**, *61*, 149–179. [[CrossRef](#)]
73. Báez, L.A.; Clancy, P. Computer Simulation of the Crystal Growth and Dissolution of Natural Gas Hydrates. *Ann. N. Y. Acad. Sci.* **1994**, *715*, 177–186. [[CrossRef](#)]
74. Parent, J.S.; Bishnoi, P. Investigations into the Nucleation Behaviour of Methane Gas Hydrates. *Chem. Eng. Commun.* **1996**, *144*, 51–64. [[CrossRef](#)]
75. Takeya, S.; Hori, A.; Hondoh, T.; Uchida, T. Freezing-Memory Effect of Water on Nucleation of CO<sub>2</sub> Hydrate Crystals. *J. Phys. Chem. B* **2000**, *104*, 4164–4168. [[CrossRef](#)]
76. Vysniauskas, A.; Bishnoi, P.R. A Kinetic Study of Methane Hydrate Formation. *Chem. Eng. Sci.* **1983**, *38*, 1061–1072. [[CrossRef](#)]
77. Sheppard, S.M.F.; Gilg, H.A. Stable Isotope Geochemistry of Clay Minerals. *Clay Miner.* **1996**, *31*, 1–24. [[CrossRef](#)]
78. McDuff, R.E. The Chemistry of Interstitial Waters, Deep Sea Drilling Project Leg 86. *Initial. Rep. Deep. Sea Drill. Proj.* **1985**, *86*, 675–687.
79. Lee, M.W.; Collett, T.S. Gas Hydrate Saturations Estimated from Fractured Reservoir at Site NGHP-01-10, Krishna-Godavari Basin, India. *J. Geophys. Res.* **2009**, *114*, 2008JB006237. [[CrossRef](#)]
80. Wei, D.; Jinqiang, L.; Zenggui, K.; Yingfeng, X.; Pin, Y. Estimation of Gas Hydrate Saturation Regarding the Hydrate Morphology in Hydrate-Bearing Sands in the Qiongdongnan Basin, South China Sea. *Pure Appl. Geophys.* **2023**, *180*, 2757–2773. [[CrossRef](#)]
81. Abid, K.; Spagnoli, G.; Teodoriu, C.; Falcone, G. Review of Pressure Coring Systems for Offshore Gas Hydrates Research. *Underw. Technol.* **2015**, *33*, 19–30. [[CrossRef](#)]
82. Yamamoto, K. Overview and Introduction: Pressure Core-Sampling and Analyses in the 2012–2013 MH21 Offshore Test of Gas Production from Methane Hydrates in the Eastern Nankai Trough. *Mar. Pet. Geol.* **2015**, *66*, 296–309. [[CrossRef](#)]
83. Lu, H.; Lorenson, T.D.; Moudrakovski, I.L.; Ripmeester, J.A.; Collett, T.S.; Hunter, R.B.; Ratcliffe, C.I. The Characteristics of Gas Hydrates Recovered from the Mount Elbert Gas Hydrate Stratigraphic Test Well, Alaska North Slope. *Mar. Pet. Geol.* **2011**, *28*, 411–418. [[CrossRef](#)]
84. Uchida, T.; Hirano, T.; Ebinuma, T.; Narita, H.; Gohara, K.; Mae, S.; Matsumoto, R. Raman Spectroscopic Determination of Hydration Number of Methane Hydrates. *AIChE J.* **1999**, *45*, 2641–2645. [[CrossRef](#)]
85. Kim, D.-Y.; Uhm, T.-W.; Lee, H.; Lee, Y.-J.; Ryu, B.-J.; Kim, J.-H. Compositional and Structural Identification of Natural Gas Hydrates Collected at Site 1249 on Ocean Drilling Program Leg 204. *Korean J. Chem. Eng.* **2005**, *22*, 569–572. [[CrossRef](#)]
86. Kida, M.; Suzuki, K.; Kawamura, T.; Oyama, H.; Nagao, J.; Ebinuma, T.; Narita, H.; Suzuki, H.; Sakagami, H.; Takahashi, N. Characteristics of Natural Gas Hydrates Occurring in Pore-Spaces of Marine Sediments Collected from the Eastern Nankai Trough, off Japan. *Energy Fuels* **2009**, *23*, 5580–5586. [[CrossRef](#)]
87. Ripmeester, J.; Lu, H.; Moudrakovski, I.; Dutrisac, R.; Wilson, L.; Wright, F.; Dallimore, S. *Structure and Composition of Hydrate in Sediment Recovered from Mallik 5L-38, Mackenzie Delta, NWT, Canada: X-ray Diffraction, Raman and Solid-State NMR Spectroscopy*; Scientific Results from the Mallik 2002 Gas Hydrate Production Research Well Program, Mackenzie Delta, Northwest Territories, Canada; Geological Survey of Canada: Vancouver, BC, Canada, 2005.
88. Lu, H.; Moudrakovski, I.; Riedel, M.; Spence, G.; Dutrisac, R.; Ripmeester, J.; Wright, F.; Dallimore, S. Occurrence and Structural Characterization of Gas Hydrates Associated with a Cold Vent Field, Offshore Vancouver Island. *J. Geophys. Res. Solid Earth* **2005**, *110*, B10204. [[CrossRef](#)]



89. Lu, H.; Moudrakovski, I.I.; Schicks, J.; Ripmeester, J.A.; Zhang, M. *The Characteristics of Gas Hydrates Recovered from Northern Cascadia Margin by IODP Expedition 311*; American Geophysical Union: Washington, DC, USA, 2006; Volume 2006, p. OS11E-08.
90. Kida, M.; Hachikubo, A.; Sakagami, H.; Minami, H.; Krylov, A.; Yamashita, S.; Takahashi, N.; Shoji, H.; Khlystov, O.; Poort, J.; et al. Natural Gas Hydrates with Locally Different Cage Occupancies and Hydration Numbers in Lake Baikal. *Geochem. Geophys. Geosyst.* **2009**, *10*, 5. [[CrossRef](#)]
91. Liu, C.; Ye, Y.; Meng, Q.; He, X.; Lu, H.; Zhang, J.; Liu, J.; Yang, S. The Characteristics of Gas Hydrates Recovered from Shenhu Area in the South China Sea. *Mar. Geol.* **2012**, *307–310*, 22–27. [[CrossRef](#)]
92. Fang, Y.; Wei, J.; Lu, H.; Liang, J.; Lu, J.; Fu, J.; Cao, J. Chemical and Structural Characteristics of Gas Hydrates from the Haima Cold Seeps in the Qiongdongnan Basin of the South China Sea. *J. Asian Earth Sci.* **2019**, *182*, 103924. [[CrossRef](#)]
93. Kida, M.; Jin, Y.; Yoneda, J.; Oshima, M.; Kato, A.; Konno, Y.; Nagao, J.; Tenma, N. Crystallographic and Geochemical Properties of Natural Gas Hydrates Accumulated in the National Gas Hydrate Program Expedition 02 Drilling Sites in the Krishna-Godavari Basin off India. *Mar. Pet. Geol.* **2019**, *108*, 471–481. [[CrossRef](#)]
94. Kang, D.; Lu, J.; Zhang, Z.; Liang, J.; Kuang, Z.; Lu, C.; Kou, B.; Lu, Q.; Wang, J. Fine-Grained Gas Hydrate Reservoir Properties Estimated from Well Logs and Lab Measurements at the Shenhu Gas Hydrate Production Test Site, the Northern Slope of the South China Sea. *Mar. Pet. Geol.* **2020**, *122*, 104676. [[CrossRef](#)]
95. Handa, Y.P. Effect of Hydrostatic Pressure and Salinity on the Stability of Gas Hydrates. *J. Phys. Chem.* **1990**, *94*, 2652–2657. [[CrossRef](#)]
96. Kneafsey, T.J.; Lu, H.; Winters, W.; Boswell, R.; Hunter, R.; Collett, T.S. Examination of Core Samples from the Mount Elbert Gas Hydrate Stratigraphic Test Well, Alaska North Slope: Effects of Retrieval and Preservation. *Mar. Pet. Geol.* **2011**, *28*, 381–393. [[CrossRef](#)]
97. Ford, K.H.; Naehr, T.H.; Skilbeck, G.C.; The Leg 201 Scientific Party. The Use of Infrared Thermal Imaging to Identify Gas Hydrate in Sediment Cores. *Proc. Ocean. Drill. Program Initial. Rep.* **2003**, *201*, 1–20.
98. Weinberger, J.L.; Brown, K.M.; Long, P.E. Painting a Picture of Gas Hydrate Distribution with Thermal Images. *Geophys. Res. Lett.* **2005**, *32*, L04609. [[CrossRef](#)]
99. Zhang, N.; Li, S.; Chen, L.; Guo, Y.; Liu, L. Study of Gas-Liquid Two-Phase Flow Characteristics in Hydrate-Bearing Sediments. *Energy* **2024**, *290*, 130215. [[CrossRef](#)]
100. Li, S.; Zheng, R.; Xu, X.; Hou, J. Natural Gas Hydrate Dissociation by Hot Brine Injection. *Pet. Sci. Technol.* **2016**, *34*, 422–428. [[CrossRef](#)]
101. Li, S.; Xu, X.; Zheng, R.; Chen, Y.; Hou, J. Experimental Investigation on Dissociation Driving Force of Methane Hydrate in Porous Media. *Fuel* **2015**, *160*, 117–122. [[CrossRef](#)]
102. Li, X.-S.; Yang, B.; Zhang, Y.; Li, G.; Duan, L.-P.; Wang, Y.; Chen, Z.-Y.; Huang, N.-S.; Wu, H.-J. Experimental Investigation into Gas Production from Methane Hydrate in Sediment by Depressurization in a Novel Pilot-Scale Hydrate Simulator. *Appl. Energy* **2012**, *93*, 722–732. [[CrossRef](#)]
103. Lee, J. Experimental Study on the Dissociation Behavior and Productivity of Gas Hydrate by Brine Injection Scheme in Porous Rock. *Energy Fuels* **2010**, *24*, 456–463. [[CrossRef](#)]
104. Oyama, H.; Konno, Y.; Masuda, Y.; Narita, H. Dependence of Depressurization-Induced Dissociation of Methane Hydrate Bearing Laboratory Cores on Heat Transfer. *Energy Fuels* **2009**, *23*, 4995–5002. [[CrossRef](#)]
105. Shankar, U.; Ojha, M.; Ghosh, R. Assessment of Gas Hydrate Reservoir from Inverted Seismic Impedance and Porosity in the Northern Hikurangi Margin, New Zealand. *Mar. Pet. Geol.* **2021**, *123*, 104751. [[CrossRef](#)]
106. Haeckel, M.; Bialas, J.; Klauke, I.; Wallmann, K.; Bohrmann, G.; Schwalenberg, K. Gas Hydrate Occurrences in the Black Sea—New Observations from the German SUGAR Project. *Fire Ice Methane Hydrate Newsl.* **2015**, *15*, 6–9.
107. Collett, T.S.; Lee, M.W.; Zyrianova, M.V.; Mrozewski, S.A.; Guerin, G.; Cook, A.E.; Goldberg, D.S. Gulf of Mexico Gas Hydrate Joint Industry Project Leg II Logging-While-Drilling Data Acquisition and Analysis. *Mar. Pet. Geol.* **2012**, *34*, 41–61. [[CrossRef](#)]
108. Komatsu, Y.; Suzuki, K.; Fujii, T. Sedimentary Facies and Paleoenvironments of a Gas-Hydrate-Bearing Sediment Core in the Eastern Nankai Trough, Japan. *Mar. Pet. Geol.* **2015**, *66*, 358–367. [[CrossRef](#)]
109. Paull, C.K.; Matsumoto, R.; Wallace, P.J.; Dillon, W.P. *Proceedings of the Ocean Drilling Program 164, Scientific Results*; Texas A & M University, Ocean Drilling Program: College Station, TX, USA, 2000.
110. Wang, X.; Collett, T.S.; Lee, M.W.; Yang, S.; Guo, Y.; Wu, S. Geological Controls on the Occurrence of Gas Hydrate from Core, Downhole Log, and Seismic Data in the Shenhu Area, South China Sea. *Mar. Geol.* **2014**, *357*, 272–292. [[CrossRef](#)]
111. Portnov, A.; Santra, M.; Cook, A.E.; Sawyer, D.E. The Jackalope Gas Hydrate System in the Northeastern Gulf of Mexico. *Mar. Pet. Geol.* **2020**, *111*, 261–278. [[CrossRef](#)]
112. Ghosh, R.; Sain, K.; Ojha, M. Effective Medium Modeling of Gas Hydrate-Filled Fractures Using the Sonic Log in the Krishna-Godavari Basin, Offshore Eastern India. *J. Geophys. Res. Solid Earth* **2010**, *115*, B06101. [[CrossRef](#)]

**Disclaimer/Publisher’s Note:** The statements, opinions and data contained in all publications are solely those of the individual author(s) and contributor(s) and not of MDPI and/or the editor(s). MDPI and/or the editor(s) disclaim responsibility for any injury to people or property resulting from any ideas, methods, instructions or products referred to in the content.